Study of non-axisymmetric divertor footprints using 2-D IR and visible cameras and a 3-D heat conduction solver in NSTX

J. W. Ahn et. al

June 11, 2012

LAWRENCE
LIVERMORE
NATIONAL
LABORATORY

Disclaimer

This document was prepared as an account of work sponsored by an agency of the United States government. Neither the United States government nor Lawrence Livermore National Security, LLC, nor any of their employees makes any warranty, expressed or implied, or assumes any legal liability or responsibility for the accuracy, completeness, or usefulness of any information, apparatus, product, or process disclosed, or represents that its use would not infringe privately owned rights. Reference herein to any specific commercial product, process, or service by trade name, trademark, manufacturer, or otherwise does not necessarily constitute or imply its endorsement, recommendation, or favoring by the United States government or Lawrence Livermore National Security, LLC. The views and opinions of authors expressed herein do not necessarily state or reflect those of the United States government or Lawrence Livermore National Security, LLC, and shall not be used for advertising or product endorsement purposes.

Study of non-axisymmetric divertor footprints using 2-D IR and visible cameras and a 3-D heat conduction solver in NSTX

J-W. Ahn*[a], K.F. Gan[b], F. Scotti[c], J.D. Lore[a], R. Maingi[a], J.M. Canik[a], T.K. Gray[a], A. McLean[d], A.L. Roquemore[c], and V. Soukhanovskii[d]

[a]*Oak Ridge National Laboratory, Oak Ridge, TN 37831, USA*

[b]*Institute of Plasma Physics, Chinese Academy of Sciences, Hefei, People's Republic of China*

[c]*Princeton Plasma Physics Laboratory, Princeton, NJ 08543, USA*

[d]*Lawrence Livermore National Laboratory, Livermore, CA 94551, USA*

Abstract

Toroidally non-axisymmetric divertor profiles during the 3-D field application and for ELMs are studied with simultaneous observation by a new wide angle visible camera and a high speed IR camera. A newly implemented 3-D heat conduction code, TACO, is used to obtain divertor heat flux. The wide angle camera data confirmed the previously reported result on the validity of vacuum field line tracing on the prediction of split strike point pattern by 3-D fields as well as the phase locking of ELM heat flux to the 3-D fields. TACO calculates the 2-D heat flux distribution allowing assessment of toroidal asymmetry of peak heat flux and heat flux width. The degree of asymmetry (DoA) is defined to quantify the asymmetric heat deposition on the divertor surface and is found to have a strong positive dependence on peak heat flux.

Corresponding Author Address: Princeton Plasma Physics Laboratory, Princeton, NJ 08543, USA

Corresponding Author e-mail: jahn@pppl.gov

Presenting Author: Joon-Wook Ahn

Presenting Author e-mail: jahn@pppl.gov

1. Introduction

Recent studies show that the axisymmetry of divertor flux profiles can be broken in the case of applying 3-D magnetic perturbations [1,2,3,4] as well as during the ELMs [5]. In these studies, the use of 2-D infrared (IR) camera plays a vital role in obtaining surface temperature data and for the derivation of heat flux profiles. However, there are two caveats in this approach to study asymmetric divertor flux profiles. First, the viewing extent of the IR camera is often limited and therefore one depends on a relatively narrow extent of the view to the whole toroidal angle (Φ) unless there are more cameras at other toroidal locations. Second, heat conduction equation solvers for the divertor heat flux profile, such as THEODOR [6], are usually in 2-D, *i.e.* 1-D in the direction of the tile depth, and 1-D along the radial extent of the plasma facing surface. The obtained heat flux profile is therefore only 1-D, *i.e.* in the radial direction (r) chosen at a particular toroidal location. These two caveats significantly restrict the capability of investigating toroidal asymmetry in the divertor flux profiles. For example, one can only compare the measured heat flux profile to that from modeling for a limited range of toroidal angles. The first caveat can be overcome by the use of a wide angle camera. This is especially feasible in the compact geometry of a spherical tokamak (ST). Furthermore, the use of 3-D heat conduction solver can provide the capability of calculating heat flux profile for the full 2-D plane.

Two wide angle visible cameras were installed on NSTX in 2010 to provide full toroidal and radial coverage of the divertor surface [7]. 2-D images from them have been used to study the effect of applied 3-D fields and ELMs on the divertor flux profiles. We also implemented a 3-D heat conduction solver, TACO [8], to obtain 2-D heat flux profiles including the effects of thin surface films on the heat flux calculation [9].

2. Experimental setup

Experiments were conducted in ELM-free and ELMy H-mode plasmas. The toroidal magnetic field (B_t) at the magnetic axis was fixed at ~0.4 T, and the neutral beam injected power (P_{NBI}) of 2-5 MW was used. Plasmas were highly shaped (elongation κ ~ 2.0-2.4, triangularity δ ~ 0.5-0.8), and the plasma current was 600-800 kA. The equilibrium was maintained as a lower single-null with the direction of the *B*-field was for the ion ∇B drift to move towards the primary X-point. Figure 1(a) shows the poloidal cross section of NSTX showing the location of diagnostic views as well as the external 3-D field coils. 3-D field pulses in NSTX are applied using a midplane coil set. In the experiments discussed here, these coils have been configured to apply n=1 or n=3 perturbative magnetic fields. The coil current was maintained at I_{3-D}=0.5 kA, which is lower than the ELM triggering level, resulting in $\delta B/B$ ~ 0.05 % for the integrated δB over the coil surface. Figure 1(b) shows the image of lower divertor plates viewed by the wide angle visible camera and figure 1(c) is the remapped image to the (r, Φ) plane with the spatial coverage of the IR and D_a cameras overlaid.

3. Divertor footprints during the 3-D field application

A. Measured heat flux profiles and comparison with wide angle images

Figure 2(a) shows the radial heat flux profile measured at the toroidal location indicated by the vertical line at Φ ~135° in figure 2(b), during the application of the n=1 3-D field. The wide angle visible camera used LiI filter (λ=670.9 nm) which has been found to best resolve fine structures at the divertor surface. The remapped wide angle visible image, figure 2(b), clearly shows the asymmetric divertor footprint and the local peak at r~46 cm in the heat flux profile, representing one of the split strike points induced by the n=1 perturbation fields. Computed vacuum field line tracing was performed to obtain connection

lengths (L_c) on the divertor surface and to compare the result to the wide angle camera images. Figure 2(c) shows that the agreement with the image data is excellent; the radial and toroidal variation of L_c well represents the observed spatial distribution of LiI emissivity in figure 2(b). This data confirms the conclusion of previous works [3,4] that the vacuum field line tracing reproduces the divertor footprints well in NSTX.

B. Divertor footprints during the ELMs triggered by 3-D field application

One of other primary observations for the divertor footprints during 3-D field application is that the heat flux profile from ELMs triggered by applied 3-D fields follows the imposed field structure [2,10]. That is, the spatial heat deposition during the triggered ELMs is 'phase locked' to the external 3-D fields. By applying the remapping technique of wide angle images for the divertor footprints of the triggered ELMs, the phase locking is also reconfirmed for both n=1 and n=3. Figure 3 illustrates the agreement between images before and during an ELM with n=1 applied. It is shown that the structure of asymmetric divertor footprint before the ELM is maintained during the ELM even with significantly stronger emission intensity. Note that the emission intensity for figure 3(b) was reduced to the level of 3(a) for a more direct comparison.

4. Analysis of asymmetric divertor heat flux for ELMy plasmas with no 3-D field application

A. TACO 3-D heat conduction solver

TACO has been implemented for use on NSTX to calculate heat flux at the divertor surface for full 2-D plane. This provides a significant advantage over 1-D radial profile particularly in the study of toroidal distribution of heat deposition. We also incorporated the thin surface film correction applied in THEODOR [6] into the process of solving heat

conduction equation [9]. A heat transmission coefficient, α, of 60 kWm^{-2}K^{-1} was found to best account for poor surface layer adhesion to the tile substrate. This value was used for all analysis presented in this paper. The 2-D heat flux data calculated by TACO was remapped to r and Φ, as was done for the wide angle visible images. This allowed for the evaluation of peak heat flux q_{peak} and heat flux width λ_q for each toroidal angle, which in turn generates a toroidal array of these quantities at each time slice. Here, we used the definition of integral λ_q used in [11], *i.e.* $\lambda_q = P_{div}/\left(2\pi r_{peak}^{div} q_{peak}^{div}\right)$.

B. Toroidal asymmetries in peak heat flux and heat flux width

In order to quantify how asymmetric the toroidal distribution of q_{peak} and λ_q is, the toroidal degree of asymmetry (DoA) for q_{peak} and λ_q, representing the full 2-D plane monitored by the IR camera, as a function of time was defined as $DoA(q_{peak}) = \sigma_{qpeak}/\bar{q}_{peak}$ and $DoA(\lambda_q) = \sigma_{\lambda q}/\bar{\lambda}_q$. Here, σ is the standard deviation of q_{peak} and λ_q over data in the toroidal array. This value is normalized by mean values of q_{peak} and λ_q respectively to produce a DoA value at each time slice. Here, $\bar{q}_{peak}$ and $\bar{\lambda}_q$ is the average over values along the toroidal direction. In case of ELMs, the helical heat deposition produces strong toroidal asymmetry for both q_{peak} and λ_q and therefore generates additional scatter of data around the mean value to the background scatter level.

An example of temporal evolution of $\bar{q}_{peak}$ and $\bar{\lambda}_q$ for a type-III ELMy discharge is given in figure 4(a). Note that $\bar{\lambda}_q$ drops during the ELMs while $\bar{q}_{peak}$ jumps. Although the decrease of λ_q during the ELM is opposite to the modest ELM broadening of heat flux width reported from some other machines [12], the deposited ELM power rapidly increases and peaks at the same time as that for the peak heat flux. Figure 4(b) shows the temporal evolution of the DoA for both q_{peak} and λ_q and it is seen that both asymmetries jump with the rise of peak heat flux. It is interesting to note that DoA(λ_q) increases during the ELM even though λ_q

5

itself decreases. Probing dependence of parameters on the peak heat flux value at ELM peak times revealed that heat flux width decreases with increasing peak heat flux (see figure 4(c)). On the other hand, DoA for q_{peak} and λ_q increases with increasing $\bar{q}_{peak,ELM}$, although the rate of increase slows down with rising $\bar{q}_{peak,ELM}$. The absolute value of DoA(q_{peak}) is always greater than DoA(λ_q) and the ratio DoA(q_{peak})/DoA(λ_q) is typically ~2-3.

The dependence of the DoA on the period within an ELM cycle was also investigated for type-I ELMy H-mode. It is found that the dependence of both DoA(q_{peak}) and DoA(λ_q) on $\bar{q}_{peak}$ is similar to the case of type-III ELMs. That is, they become largest at the ELM peak times and DoA(q_{peak}) can be as high as ~1.4 while DoA(λ_q) can reach up to ~0.5 for the dataset examined. Both DoA values increase with increasing q_{peak} and therefore the degree of asymmetric heat deposition is highest at the ELM peak times, while it becomes lower toward the later stage of the inter-ELM period. This dependence of asymmetric heat deposition on the ELM cycle also appears to be related to the absolute value of peak heat flux. That is, higher peak heat flux leads to stronger degree of asymmetric q_{peak} and λ_q. It is also found that the correlation between DoA(q_{peak}) and DoA(λ_q) is the strongest at ELM peak times and becomes weaker later in the ELM cycle.

5. Discussion and Summary

The study of divertor heat and particle deposition can be more comprehensively carried out by making use of a wide angle image diagnostic. While the conventional 1-D flux profile at a specific toroidal location can still provide valuable information, the full 2-D image can significantly improve data analysis and comparison with modeling. The compact ST geometry of NSTX makes the coverage of toroidal extent almost full by a single wide angle visible camera and this turns out very efficient to investigate divertor footprint patterns during the 3-D field application or ELMs.

While the present NSTX fast IR camera does not provide toroidal coverage approaching that of the visible cameras, the view is significantly wider than similar instruments on conventional tokamaks. TACO can directly produce 2-D heat flux data and this has been used to study toroidal asymmetry of heat flux. The degree of asymmetry (DoA) was defined here to quantify how asymmetrically q_{peak} and λ_q are distributed over the whole monitored divertor surface at a given time slice. Although the choice of $\alpha=60$ kWm^{-2}K^{-1} was based on the energy conservation, it is not clear how accurately this value can take account of real surface film effect and therefore the impact of this uncertainty on the behavior of DoAs is yet to be investigated.

Acknowledgements

References

[1] O. Schmitz, T.E. Evans, M.E. Fenstermacher, et al. Plasma Phys. Control. Fusion **50** (2008) 124029

[2] M.W. Jakubowski, T.E. Evans, M.E. Fenstermacher, et al. Nucl. Fusion **49** (2009) 095013

[3] J-W. Ahn, J.M. Canik, V.A. Soukhanovskii, et al. Nucl. Fusion **50** (2010) 045010

[4] J-W. Ahn, R. Maingi, J.M. Canik, et al. Phys. Plasmas **18** (2011) 056108

[5] T. Eich, A. Herrmann, J. Neuhauser, et al. Plasma Phys. Control. Fusion **47** (2005) 815

[6] A. Herrmann, W. Junker, K. Günther et al. Plasma Phys. Control. Fusion **37** (1995) 17

[7] F. Scotti, "Full toroidal imaging of non-axisymmetric plasma material interaction in the National Spherical Torus eXperiment divertor", submitted to Rev. Sci. Instrum. (2012)

[8] G. Castle, "Theory and Operating Instructions for the taco_run code", COMPASS Note 97.16, UKAEA Fusion (1997)

[9] K.F. Gan, "2D divertor heat flux distribution using a 3-D heat conduction solver in NSTX", to be submitted to Rev. Sci. Instrum.

[10] J-W. Ahn, J.M. Canik, R. Maingi, et al. J. Nucl. Mater. **415** (2011) S918

[11] A. Loarte, S. Bosch, A. Chankin, et al. J. Nucl. Mater. **266-269** (1999) 587

[12] A. Herrmann, T. Eich, S. Jachmich, et al. J. Nucl. Mater. **313-316** (2003) 759

Figure Captions

Figure 1 Poloidal cross section of NSTX (*a*) with magnetic equilibrium reconstruction, field of view of the IR, D_α, and wide angle visible cameras and the location of external 3D field coil overlaid. Figure (*b*) shows the raw image of lower divertor plates viewed by the wide angle visible camera, which is remapped to the (r, Φ) plane as in figure (c)

Figure 2 Comparison of 1-D heat flux profile from the IR measurement (a) with the remapped 2-D wide angle visible camera image using a LiI filter (λ=670.9nm) (b), during the n=1 magnetic perturbation. Figure (c) is the contour plot of calculated connection lengths for the same time slice.

Figure 3 Images of wide angle visible camera for lower divertor plates during the n=1 3-D field application, remapped from (x, y) to (r, Φ) plane. The upper image is before the ELM and the lower one is during the ELM, triggered by n=1 magnetic perturbation. The light intensity for the ELM case (lower image) was reduced for clearer comparison.

Figure 4 Temporal evolution of mean q_{peak} and λ_q (a) as well as of DoA for each quantity (b). Figures (c) and (d) show the dependence of average λ_q and DoAs, respectively, on q_{peak}.
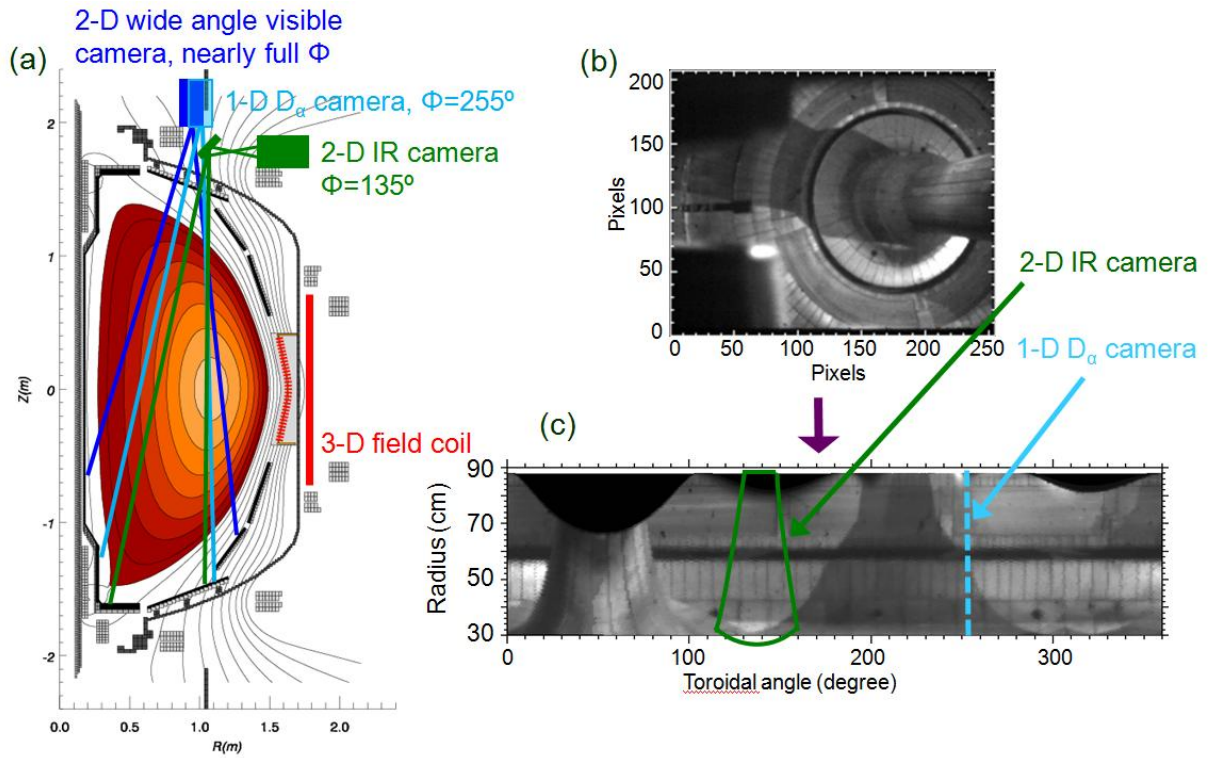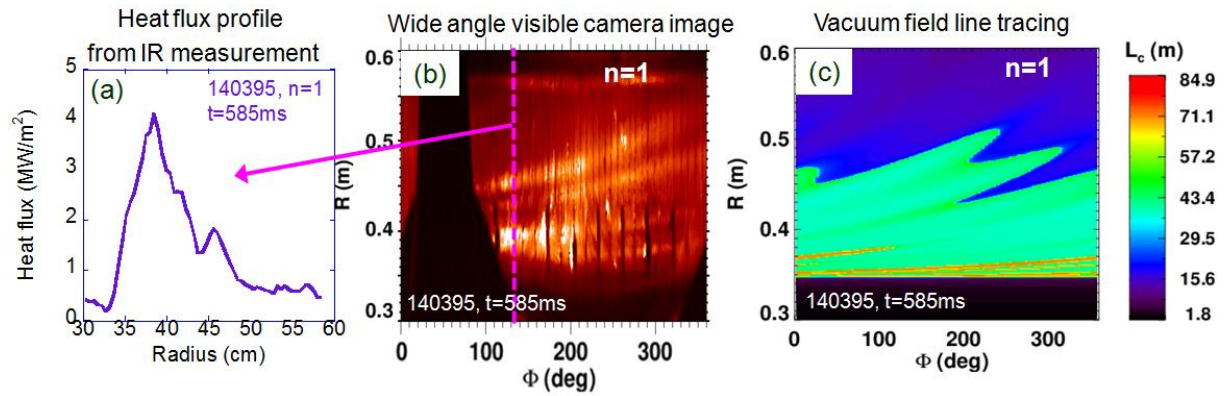
Figures

Figure 1:

Figure 2:

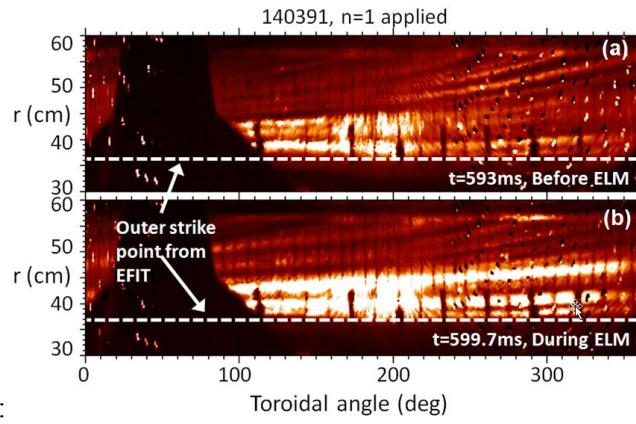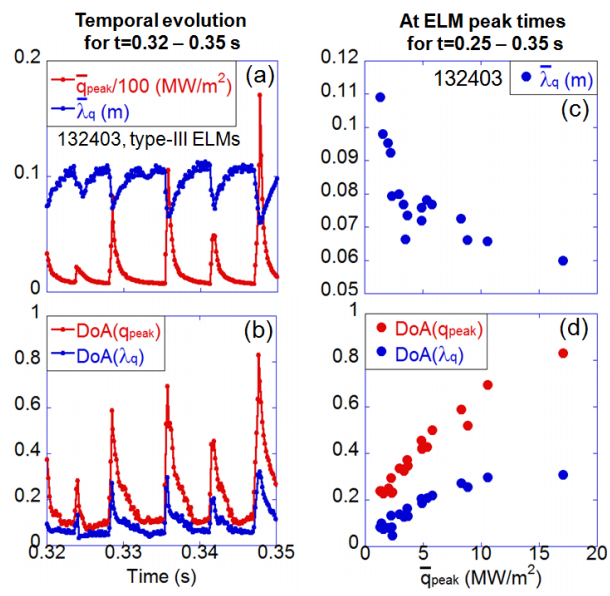Figure 3:

Figure 4: